Photocatalytic degradation of ketorolac tromethamine (KTC) drug in aqueous phase using prepared Ag-doped ZnO microplates

Amandeep Kaur[1], Alex O Ibhadon[2] and Sushil Kumar Kansal[1*]

[1]Dr. S.S. B. University Institute of Chemical Engineering and Technology, Panjab University, Chandigarh

[2]Department of Chemical Engineering, School of Engineering, University of Hull, Cottingham Road, Hull, United Kingdom HU6 7RX

Abstract

In this study, Ag-doped ZnO microplates were prepared via precipitation technique and further characterized by FESEM, EDS, XRD, FTIR, TGA, XPS, UV-DRS and RT-PL techniques. The outcomes indicated that Ag^+ ions were well incorporated into ZnO lattice leading to the absorption of ZnO in visible region as well as effective charge separation. The photocatalytic experiments showed that Ag-doped ZnO microplates show higher catalytic activity (91%) than bare ZnO (71%) for the degradation of KTC drug under solar illumination. The photocatalytic degradation of KTC drug over Ag doped ZnO microplates obeyed pseudo first-order kinetics model. Also, the role of active species was examined by the addition of several scavengers in the photocatalytic degradation system. The results indicated that h^+, $^{\bullet}OH_s$, $^1O_2$ and $^{\bullet}OH$ were considered as prime reactive species in photocatalytic degradation process.

Keywords: Ag-doped ZnO, Strong adsorption, Ketorolac tromethamine, Solar light, Photocatalysis

Highlights

- Ag-doped ZnO photocatalyst have been synthesized using precipitation method
- Ag-doped photocatalyst showed excellent photocatalytic activity for the degradation of ketorolac tromethamine drug
- The improved photoactivity is due to the effective charge separation

***Corresponding authors**
E-mail Address: sushilkk1@yahoo.co.in; sushilkk1@pu.ac.in
Ph: +91-172-2534920(O), 09876581564 (Sushil. K. Kansal)

1. Introduction

In recent years, researchers have put significant efforts in developing methods to utilize solar energy more effectively in order to provide solution to one of the world's major problem-energy crisis. One promising approach is to synthesize highly active photocatalysts to promote water splitting, photocatalytic treatment of environment pollutants, or both under solar illumination [1-3]. Among various materials, metal oxide based nanostructures have gained considerable attention owing to their high surface to volume ratio, adjustable band gap and high stability [4-6]. ZnO has been regarded as a promising catalyst because of its low cost, non-toxic nature and high electron stability [7-9]. But, it can only be activated under UV light because of ample band gap (i.e. 3.2 eV), and more electron-hole recombination, thereby its photocatalytic efficiency is still remained at slow rate because of limited adsorption of solar light [10]. Therefore, recent research has been focused to design ZnO based photocatalysts with broad wavelength for light absorption that utilize full solar spectrum [11].

In order to achieve broad wavelength spectrum for ZnO, two common approaches are used - doping with metals (Ag, Au, Pt, etc.), non-metals (carbon, nitrogen, sulphur, etc.) and composites with lower band gap semiconductors such as CuO, CdS, Fe_2O_3, CdSe, etc. [12-16]. Among them, band-gap modification of ZnO through metal doping is considered as one of the most effective approach to broaden the absorption of light into visible region by suppressing electron-hole recombination. It was confirmed that doping with small concentration increased the life span of photogenerated charge carriers and thereby improved photocatalytic degradation efficiency [17, 18]. Recent studies have shown that silver is the best doping element because of its larger ionic size, least orbital energy and high solubility

[19]. It should be noted that not all transition metals give a positive response. In some cases, transition metals reduce the photocatalytic degradation efficiency because of increase in electron-hole recombination.

Herein, we report a precipitation method to prepare Ag-doped ZnO photocatalyst. The as-prepared materials were further characterized using many techniques to examine their compositional, morphological, optical and luminescent behaviour. The activity of the photocatalyst was studied for the degradation of a biorecalcitrant organic pollutant, ketorolac tromethamine (KTC) under solar irradiation. Also, the impact of pH and catalyst loading on degradation efficiency was examined.

2. Experimental section

2.1. Materials and methods

Zinc acetate dehydrate (≥ 98% purity), silver nitrate (≥ 99% purity), sodium hydroxide (> 97% purity), sodium azide (≥ 99.5% purity), sodium chloride (≥ 99% purity) and potassium iodide (≥ 99% purity) were procured from Merck, India. Isopropanol (99% purity) was obtained from SD Fine Chem Limited, India. Ketorolac tromethamine (KTC) was provided by Saurav Chemicals Limited, Derabassi, India. Double distilled water (DDW) was utilized to brew all stock solutions and reagents were used as received. 0.1 N solutions of HCl and NaOH were added to regulate the pH of KTC solution with Mettler Toledo pH-meter.

Ag-doped ZnO photocatalyst was synthesized using similar precipitation method as reported earlier [20]. To synthesize Ag-doped ZnO, firstly, 0.05 moles of zinc acetate dihydrate were mixed in 50 mL double distilled water. Subsequently, 1M NaOH aqueous solution was added dropwise to achieve the pH of the suspension to about pH 12. After that, 0.025 % of $AgNO_3$ was dissolved in ethanol-water mixture (1:1) and then added dropwise into above solution and stirred for 16 hours. The obtained precipitates was washed thoroughly with ethanol and then with DDW, filtered and finally dried in an oven at 80 °C for overnight. Pure ZnO was also obtained using same procedure except adding up $AgNO_3$ salt.

2.2. Characterization

The morphology of prepared catalyst was examined using field emission scanning electron microscope (Hitachi-8010). The structure and crystallinity of synthesized samples was examined on powder X-ray diffraction (PXRD) instrument. The scan analysis was operated within 2θ range of 10-80° by Cu kα radiation. Fourier transform infrared (FTIR) spectra of samples were obtained from Thermofisher Nicolet iS50 spectrometer in the range of 400-4000 cm^{-1}. TGA analysis was conducted on Perkin Elmer STA 6000 instrument using nitrogen gas with a heating rate of 10 °C per minute. The chemical composition and electronic states of samples were scrutinized on X-ray photoelectron spectroscopy (XPS) with monochromated Mg Kα X-ray (hν = 1253.6 eV) radiation. UV-vis diffuse reflectance (DRS) of samples was carried out on UV-vis (Shimadzu, UV-2600) spectrophotometer using $BaSO_4$ as reference. Room temperature photoluminescence (RT-PL) spectra of samples were obtained using fluorescence spectrophotometer (Hitachi F-7000) at an excitation wavelength of 340 nm.

2.3. Photocatalytic experiments

The photocatalytic activity of Ag doped ZnO was tested by degrading the KTC under solar light irradiation (65-70 K lux, recorded on CHY 332 light meter). In a photocatalytic experiment, 0.25 g of as-synthesized photocatalyst was dispersed into 100 mL of aqueous solution of KTC drug. Adsorption-desorption equilibrium is accomplished in 30 minutes in dark prior to light illumination to initiate the degradation reaction. Then, 2 mL aliquot was extracted at specific time periods and filtered through 0.45 μm Chromafil syringe filter. The absorbance of filtrate was measured using UV-vis Systronics-2202 spectrophotometer and degradation efficiency was computed as:

Degradation efficiency = $[1-(C/C_0)] \times 100$ (1)

where C_0 is the initial KTC concentration and C is KTC concentration after irradiating with solar light at a certain time.

3. Results and discussion

3.1. Characterization of Ag-doped ZnO powder

The electrode morphologies of Ag doped ZnO was observed using scanning electron microscope (FESEM) and typical electron micrographs are shown in **Fig. 1**. As seen from **Fig. 1** (a-d), the prepared sample consists of 2-D plate like morphology and grown in high density. **Fig. 1**(b) and (d) exhibits the high resolution images which verified that microplates are formed by accretion of hundreds of nanoparticles. The typical thickness of plates is 40-50 nm and sizes are in the range of micrometers. EDS spectrum (**Fig. 1** (e)) of Ag doped ZnO identifies the existence of Ag in synthesized sample. XRD pattern of as-prepared ZnO and Ag-doped ZnO are shown in **Fig. 1** (f). In case of ZnO, all the diffraction peaks are well matched with JCPDS data card no. 36-1451. XRD studies reveal that ZnO and Ag doped catalysts exhibits various well defined peaks of wurtzite hexagonal ZnO. In **Fig. 1** (f), the diffraction peaks observed at 2θ = 31.74°, 34.47°, 36.42°, 47.53°, 56.68°, 62.88°, 66.43°, 67.92°, 69.18°, 72.60° and 77.19° can be related to the crystal planes of (100), (002), (101), (102), (110), (103), (200), (112), (201), (004) and (202), respectively [21,22]. The peak corresponds to (101) is more intense than other peaks and shows very small shifts towards decreasing 2θ value with Ag doping. The slight increase in intensities of all the peaks for Ag doping (0.025%) indicates improved crystallinity of ZnO [23]. No diffraction peak allied to Ag is detected that can be due to very small concentration of Ag^+ ions in sample, which confirms the replacement of Zn^{2+} by Ag^+ ions into ZnO matrix. The crystallite sizes of the prepared samples are calculated from Debye Scherer's equation.

$D = 0.9\lambda/\beta \cos\theta$ (2)

where λ is the wavelength of the X-ray light, β is the broadening of diffraction peak at FWHM and θ is Bragg's angle. The lattice constants 'a' and 'c' are estimated from following equation:

$$\frac{1}{d^2} = \frac{4}{3}\left[h^2 + hk + \frac{k^2}{a^2}\right] + \frac{l^2}{c^2} \tag{3}$$

The lattice constants for ZnO and doped ZnO are a = 3.239Å, c = 5.197Å and a = 3.251 Å, c= 5.201 Å, respectively. The crystallite size of pristine and doped ZnO is estimated as 38.45 nm and 34.15 nm respectively. The values of lattice parameters are increased with the doping which is due to the inclusion of Ag^+ ions into ZnO lattice or substitution of Zn^{2+} with Ag^+ ions because of larger difference in radius of Zn^{2+} (0.074 nm) and Ag^+ (0.126 nm) ions [24].

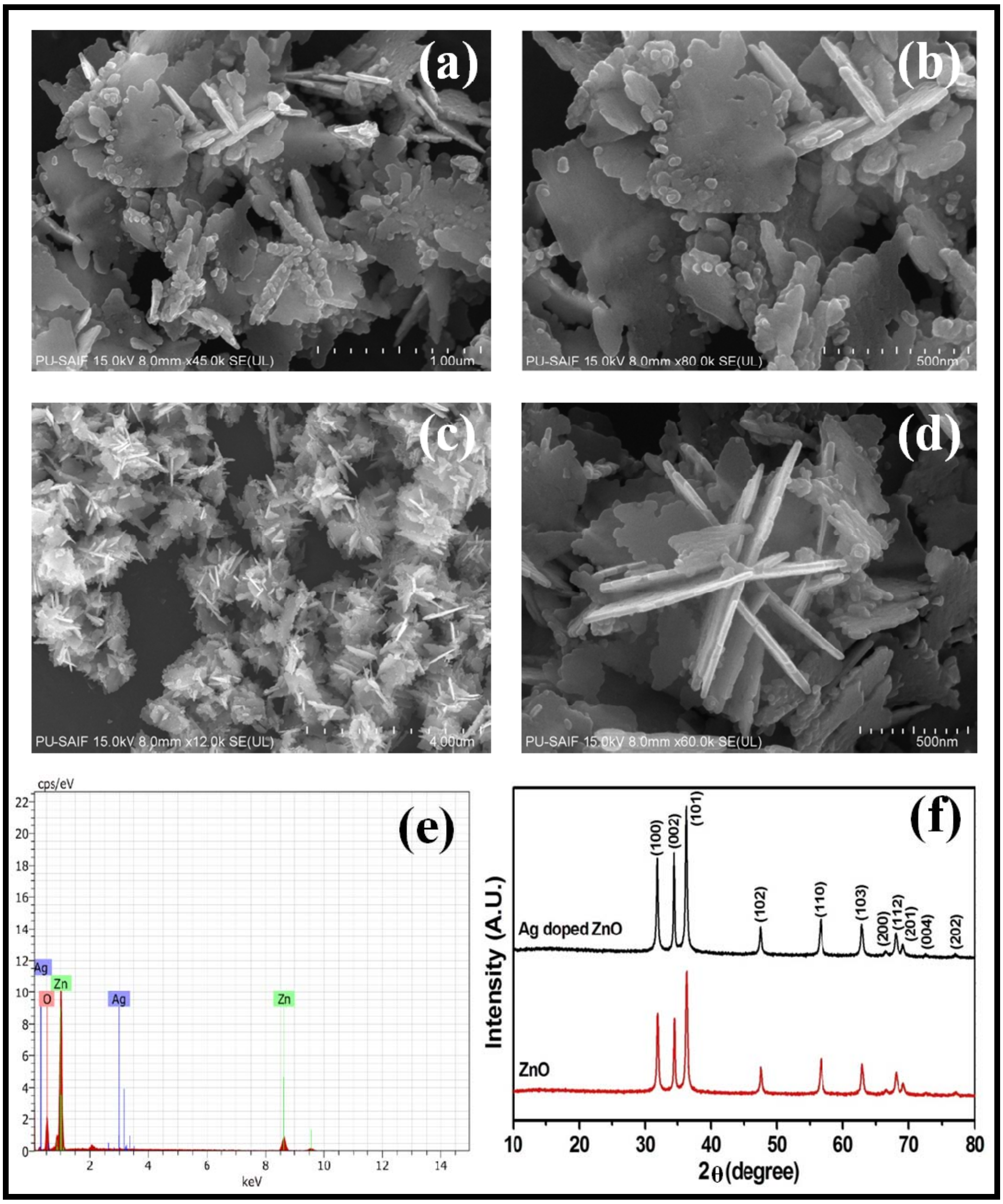

Fig.1. FESEM images (a), (c) at low resolution, (b), (d) at high resolution (e) EDS and (d) XRD of Ag doped ZnO microplates

The as-prepared products were examined in terms of their atomic and molecular vibration. The FTIR spectrum of Ag-doped ZnO sample was obtained in the range of wavenumber 400-4000 cm^{-1} which followed the similar pattern as that of pristine ZnO and as shown in **Fig 2**. The peak at 3373 cm^{-1} corresponded to the absorption of surface hydroxyl groups [25, 26]. The broad band positioned at 560 cm^{-1} and 876 cm^{-1} ascribed to the stretching vibrations of Zn-O [27]. It was inferred that the shift in band position could be as a result of introduction of Ag^+ ions into ZnO matrix. From the TGA analysis, it was seen that the total weight loss (%) for Ag-doped ZnO and ZnO microplates were found to be 6.4 % and 5.3% respectively, in the range of 0 to 800 ^{0}C. The initial weight loss for both samples up to 500 °C was due to the evaporation of physically and chemically adsorbed water molecules on the surface of microplates [28-30]. But, the weight loss at higher temperature (500-800 °C) was about 0.5% and 1.2% for ZnO and Ag doped ZnO respectively, which depicts thermal stability of prepared samples.

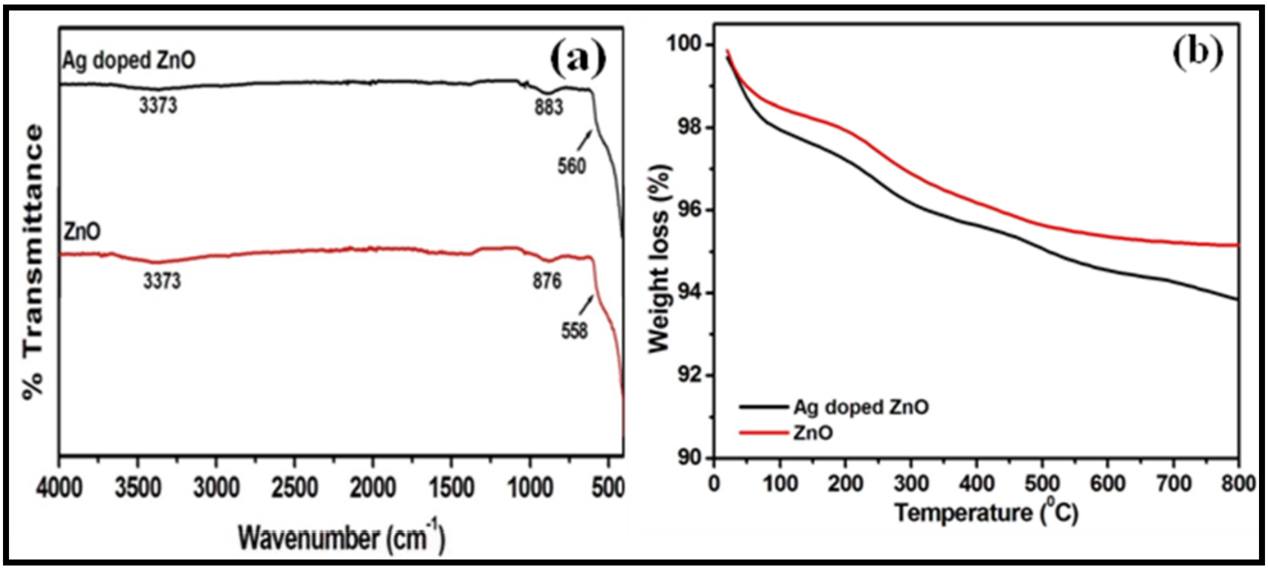

Fig. 2. (a) FTIR spectra (b) TGA of ZnO and Ag-doped ZnO microplates

Surface composition of the silver doped ZnO microplates were investigated by X-ray photo electron spectroscopy. **Fig. 3** (a)-(e) displays the scan survey spectra of Ag doped ZnO and all the peaks on the curve may be corresponded to Zn, Ag, O and C element, while C 1s at 284.8 eV is because of adventitious hydrocarbon (**Fig. 3** (d)) from instrument itself. **Fig. 3** (a) exhibits the Zn 2p binding energy region. The Zn $2p_{3/2}$ and $2p_{½}$ spin orbital states for sample is positioned at binding energy of 1023.0 eV and 1045.6 eV, respectively [31, 32]. As observed from high resolution Ag 3d spectrum (**Fig. 3** (b)), Ag-doped ZnO exhibited twice peaks identified at 365.5 eV and 372.7 eV were corresponding to Ag $3d_{5/2}$ and Ag $3d_{3/2}$

respectively [33, 34]. These values are well agreement with metallic silver values [35, 36]. In O 1s spectrum (**Fig. 3** (c)), peak obtained at binding energy 529.7 eV ascribed to the lattice oxygen of ZnO. The peaks found in overall XPS spectrum (**Fig. 3** (e)) were in accordance with the earlier results [37].

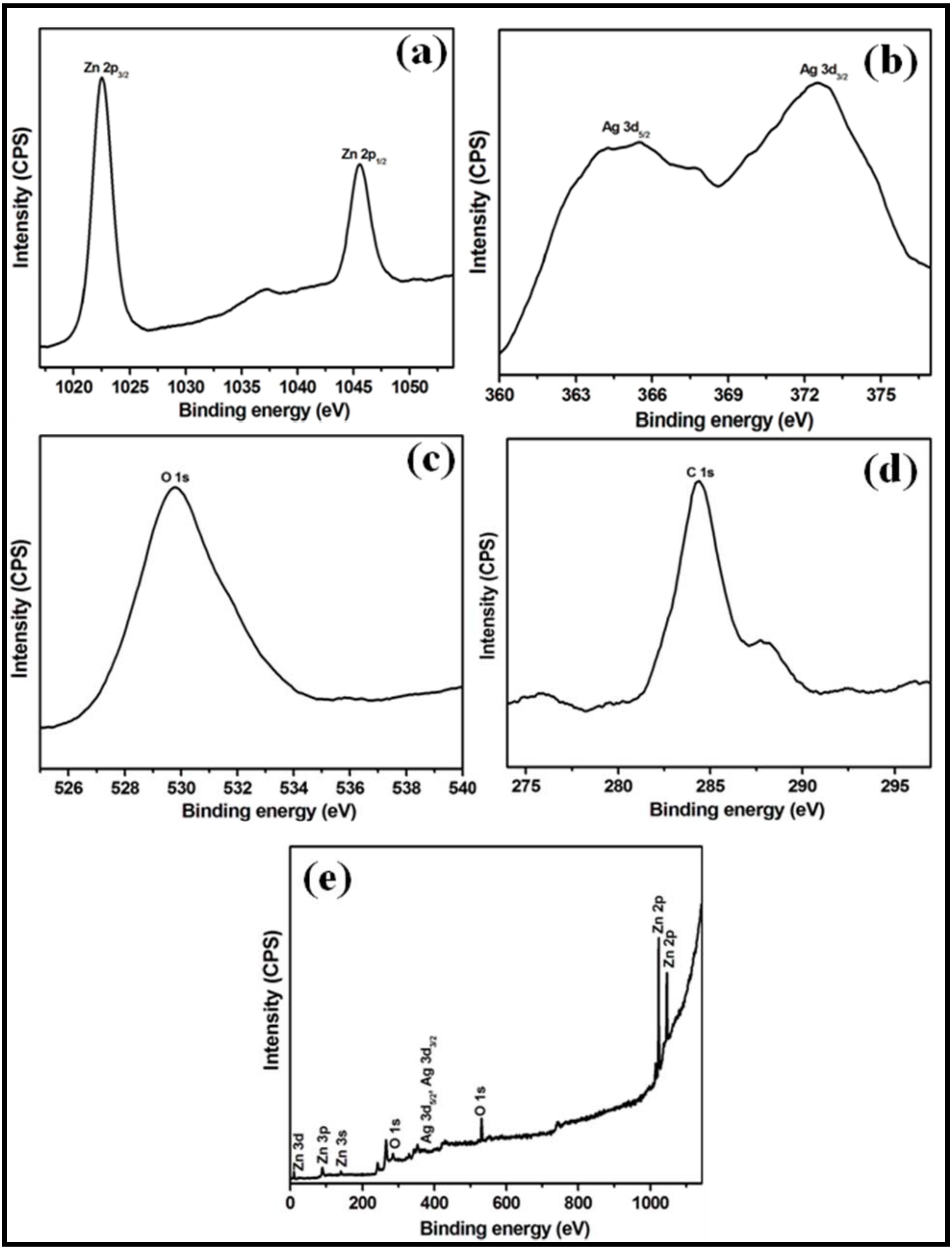

Fig. 3. XPS spectra of Ag-doped ZnO microplates for (a) Zn 2p; (b) Ag 3d; (c) O 1s; (d) C 1s and (e) Full spectrum.

UV-vis DRS experiment was carried out to examine the light absorbed by prepared catalyst. The UV-vis spectra of the Ag-doped ZnO and ZnO catalysts are shown in inset of **Fig. 4** (a). The synthesized Ag doped ZnO sample showed absorption of light shifted to a longer wavelength region as compare to bare ZnO. A classical Tauc method was further used to estimate the energy band gap of ZnO and Ag doped ZnO samples according to given equation [38]:

$$(\alpha h\nu)^n = A\ (h\nu - E_{bg}) \quad (2)$$

where α, h, ν, E_{bg} and A are absorption coefficient, planck constant, light frequency, band gap and constant respectively. Among them, n is calculated from the optical transmission of a semiconductor. The value of n for Ag doped ZnO and ZnO are taken as 2, because of the characteristic of direct band transition. Thus, the energy band gap of ZnO and Ag doped ZnO can be computed from a plot of $(\alpha h\nu)^2$ versus hν, (**Fig 4** (a)), and were found to be 3.18 eV and 3.10 eV, respectively. Furthermore, the substitution of silver ions into Zn^{2+} sites showed red shift in band gap absorption of ZnO microplates as reported in literature [39].

Optical properties of prepared catalysts were monitored using RT-PL at an excitation wavelength of 340 nm and results were shown in **Fig. 4** (b). The PL spectrum of ZnO possesses major UV-emission peak at 392 nm is because of the extinction of excitons and visible light luminescence bands centred at 427 nm and 467 nm was ascribed due to the high density of surface defects, oxygen vacancies and the recombination of free charge carriers [36]. The green emission band centred at 528 nm is because of electron-hole recombination which occupies single ion oxygen vacancy [37]. The PL intensity of Ag-doped ZnO was reduced in contrast to pristine ZnO. The PL intensity of ZnO was significantly quenched by the substitution of Ag in ZnO matrix [40], and thus Ag-doped ZnO may show higher photocatalytic activity than ZnO catalyst.

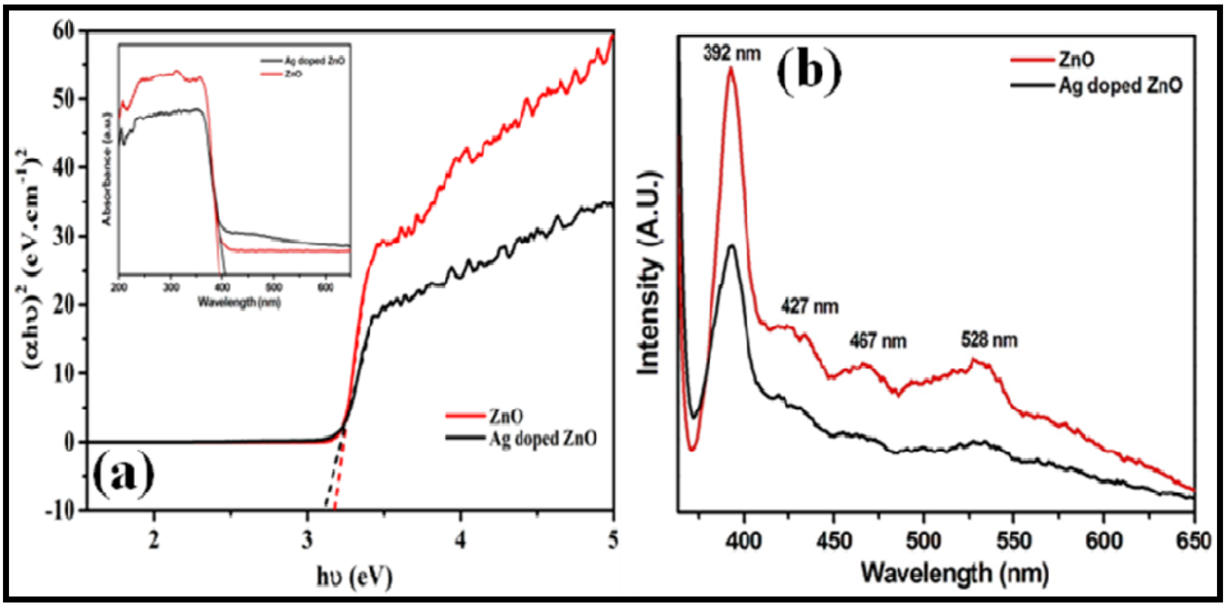

Fig. 4. (a) plot of (αhν) versus energy (hν), (inset) UV-vis DRS spectra; (b) RT-PL spectra of as-synthesized ZnO and Ag-doped ZnO microplates

3.2. Photocatalytic performance

In order to assess the photocatalytic activity of Ag-doped ZnO microplates, various degradation experiments were performed to degrade the KTC drug under solar irradiation. Ketorolac tromethamine (KTC) exhibits an absorption peak at λ_{max} = 320 nm. **Fig. 5** (a) shows photodegradation of KTC over Ag-doped ZnO microplates under solar light. It is observed that the absorbance of drug solution gets reduced during photocatalytic reaction. About 91% of KTC drug solution was degraded within 110 minutes of solar irradiation, higher than that of pristine ZnO (71%) under similar conditions. It can be examined that no considerable degradation of drug solution occurred only under solar light. However, about 32% adsorption of drug was observed on the surface of Ag-doped ZnO as shown in **Fig 5** (b).

The effect of initial drug pH on degradation efficiency with Ag-doped ZnO was studied by varying the pH of drug solution (10 mg/L) from 5 to 11, keeping all other conditions constant i.e. catalyst dose (0.25 g/L). The degradation efficiency of KTC enhanced from 80% to 91%, as pH increases from 5 to 7 and achieved maximum degradation efficiency (91%) at pH 7. On further increasing the pH from 9 to 11, degradation efficiency decreased from 90% to 88% (**Fig 5** (c)). The photodegradation efficiency of catalyst rely on the acessiblility of active sites, so it is required to optimize the catalyst dose for the degradation of drug compound.

To optimize the catalyst dose for the degradation of KTC (10 mg/L), number of experiments were performed by altering the catalyst loading from 0. 15 g/L to 0.5 g/L at pH 7. It was noticed with the increase in catalyst loading from 0.15 g/L to 0.25 g/L, the degradation efficiency of drug increased. However, as the dose was increased from 0.25 g/L to 0.5 g/L, photodegradation efficiency was decreased which could be due to the obstruction in the scattering of sunlight in hazy suspension (**Fig 5** (d)). The photocatalytic degradation of ketorolac tromethamine using Ag doped ZnO has not yet been described in literature. But, Ag doped ZnO used as photocatalyst for the degradation of other organic pollutants such as dyes and phenols [41-43]. Yildirim et al. [44] studied the photocatalytic degradation of methylene orange with Ag-doped zinc oxide nanoparticles. Authors concluded that improved photocatalytic degradation of dye was obtained with Ag-doped ZnO as compared to pristine ZnO. Complete degradation of MO dye was achieved in 90 minutes under UV light with 0.3% Ag doped ZnO. Udom et al. [45] investigated the effect of Ag concentration on removal efficiency of methyl orange and results exhibited that about 99% of methyl orange (20 mg/L) was achieved in 2 hours with 1.2% Ag-doped ZnO under UV irradiation. Another study showed 99.5% degradation of methyl orange in 60 minutes using Ag/ZnO under simulated solar light [46]. In the present work, the prepared catalyst exihibits similar results ~91% photocatalytic activity for the degradation of KTC under solar irradiation. The reaction kinetics of ketorolac tromethamine (10 mg/L, pH 7) degradation was examined with synthesized Ag-doped ZnO (0.25 g/L), using Langmuir-Hinshelwood kinetic model [17, 26].

According to which, ln $C_0/C = kt$, where C_0 is the inital concentration of drug and C is the final concentration of drug after photocatalysis at different time (t) intervals, k is the apparant rate constant and t is the degradation reaction time. **Fig 5** (e) exhibits the plot of $\ln(C_0/C)$ vs time for the photocatalytic degradation of KTC. It obeyed pseudo first order kinetic model with apparent reaction rate constant (k) of 0.02287 min^{-1}.

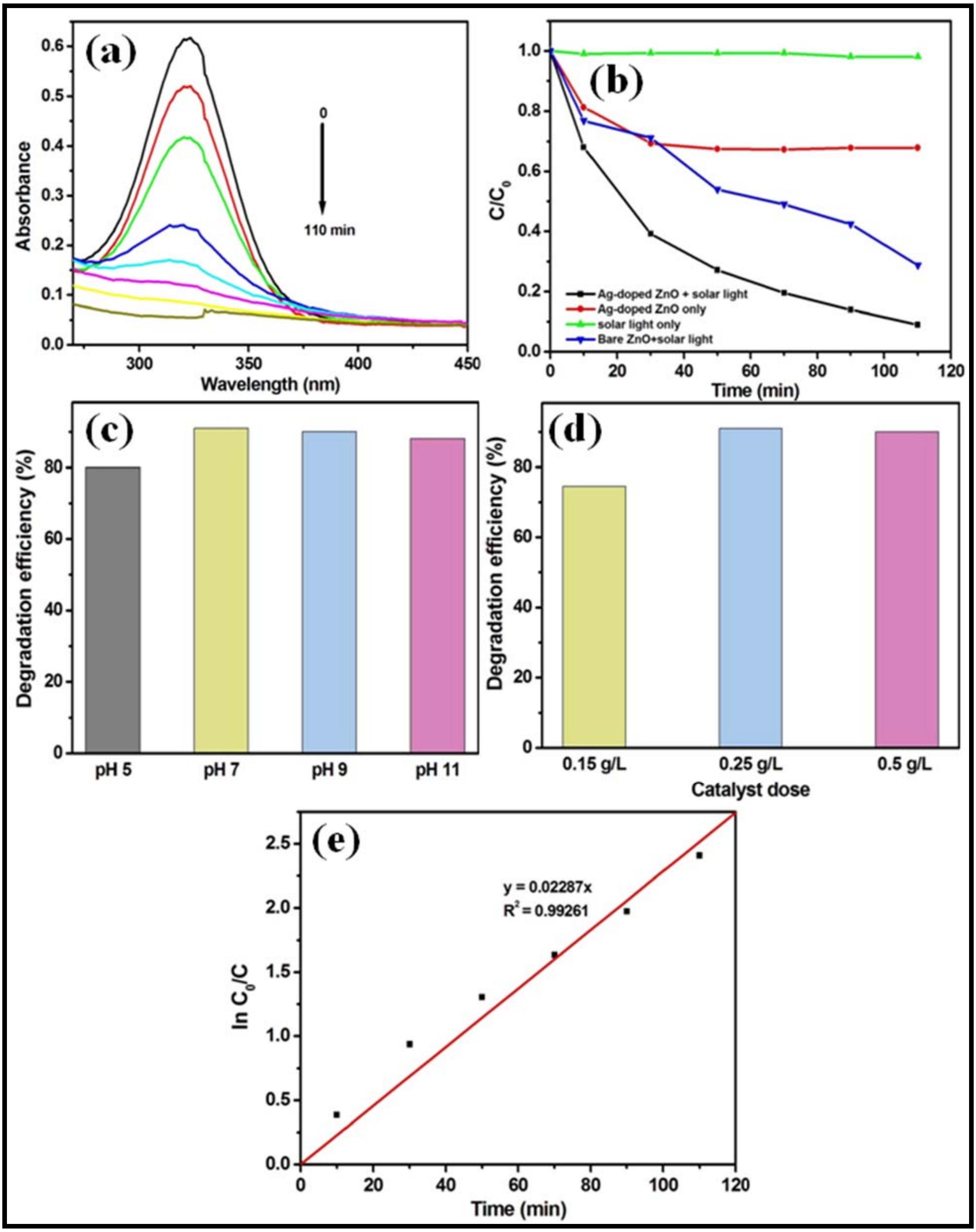

Fig. 5. (a) UV-vis absorbance spectra of KTC; (b) Comparison of photolysis, adsorption and photocatalytic activity of bare ZnO and Ag-doped ZnO under solar light (catalyst dose 0.25

g/L, drug concentration 10 mg/L, pH 7); effect of (c) pH of drug solution; (d) catalyst dose on degradation efficiency and (e) Plot of $\ln C_0/C$ vs time demonstrating photocatalytic degradation of KTC drug kinetics.

3.3. Role of primary reactive species

To determine the contribution of reactive species, various scavengers (0.01 M) were introduced into photodegradation system prior to catalyst addition. The scavengers such as potassium iodide (KI) for h^+ and $^{\bullet}OH_s$, sodium azide (NaN_3) for $^1O_2$ and $^{\bullet}OH$, sodium chloride (NaCl) for h^+ and isopropanol (IPA) for $^{\bullet}OH$ were employed in this study [47-50]. As shown in **Fig. 6**, with the addition of KI, the degradation efficiency of KTC declined to great extent, depicting that h^+ and $^{\bullet}OH_s$ plays important role in photocatalytic process. In addition, major inhibition effect on degradation performance was witnessed when NaN_3 was employed to quench $^1O_2$ and $^{\bullet}OH$ that verifies the significant role of reactive species in the photocatalytic degradation process. In addition, the photocatalytic degradation of KTC (91%) decreased to 37% and 41% after NaCl and IPA was added respectively, indicating h^+, $^{\bullet}OH_s$, $^{\bullet 1}O_2$ and $^{\bullet}OH$ are the prime reactive species in photocatalytic degradation process.

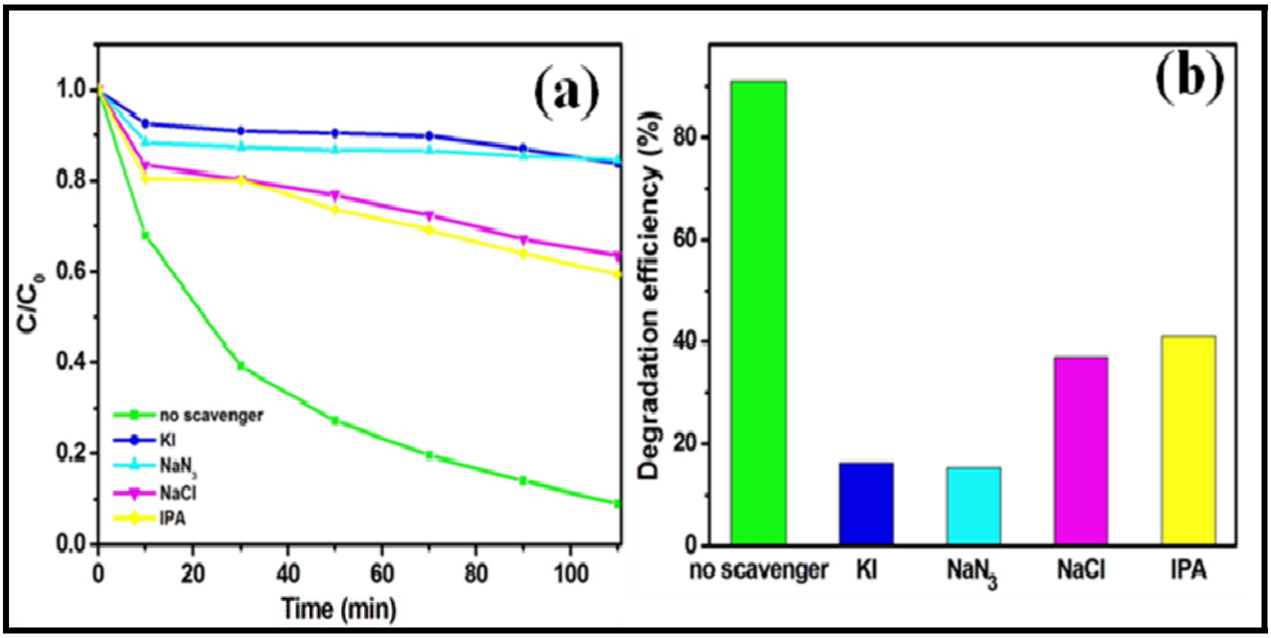

Fig. 6 (a) The extent of photocatalytic degradation and (b) degradation efficiency of the KTC solution (10 mg/L) with and without different scavengers over Ag-doped ZnO microplates

3.4. Photocatalytic degradation mechanism

The illustrative mechanism of solar light active photocatalytic reaction on the surface of Ag-doped ZnO has been shown in **Fig. 7**. When light incidents on the surface of ZnO, electrons-holes were generated in conduction and valence band, respectively (equation 5). Schottky barrier is build up at the interface of ZnO and ensuing an efficient transfer of electrons from ZnO to the newly formed interface. In dopant catalyst, the excition of electrons are effective even with lower photon energy. Maenwhile, the Ag dopant act as an electrons acceptor that traps the excited electrons from conduction band ZnO (equation 6) [50], inhibit the electron-hole recombination and thus enhancing photocatalytic efficiency [51, 52]. The photogenerated e^{-} react with O_2 to form $O_2^{\bullet-}$ (equation 7). The photogenerated holes can easily captured by ^{-}OH as well as H_2O to produce hydroxyl radicals ($^{\bullet}OH$) in equation (equation 8). The overall photocatalytic mechanism (equation 9) is based on the reaction between pollutant and generated active species ($O_2^{\bullet-}$ and $^{\bullet}OH$). Ag dopant can extend the absorption of light by enhancing the photoresponse of cation loaded ZnO in entire spectrum of solar light. However, high dopant concentration increases recombination rate of photoexcited charge carriers and thereby decreasing photodegradation efficiency.

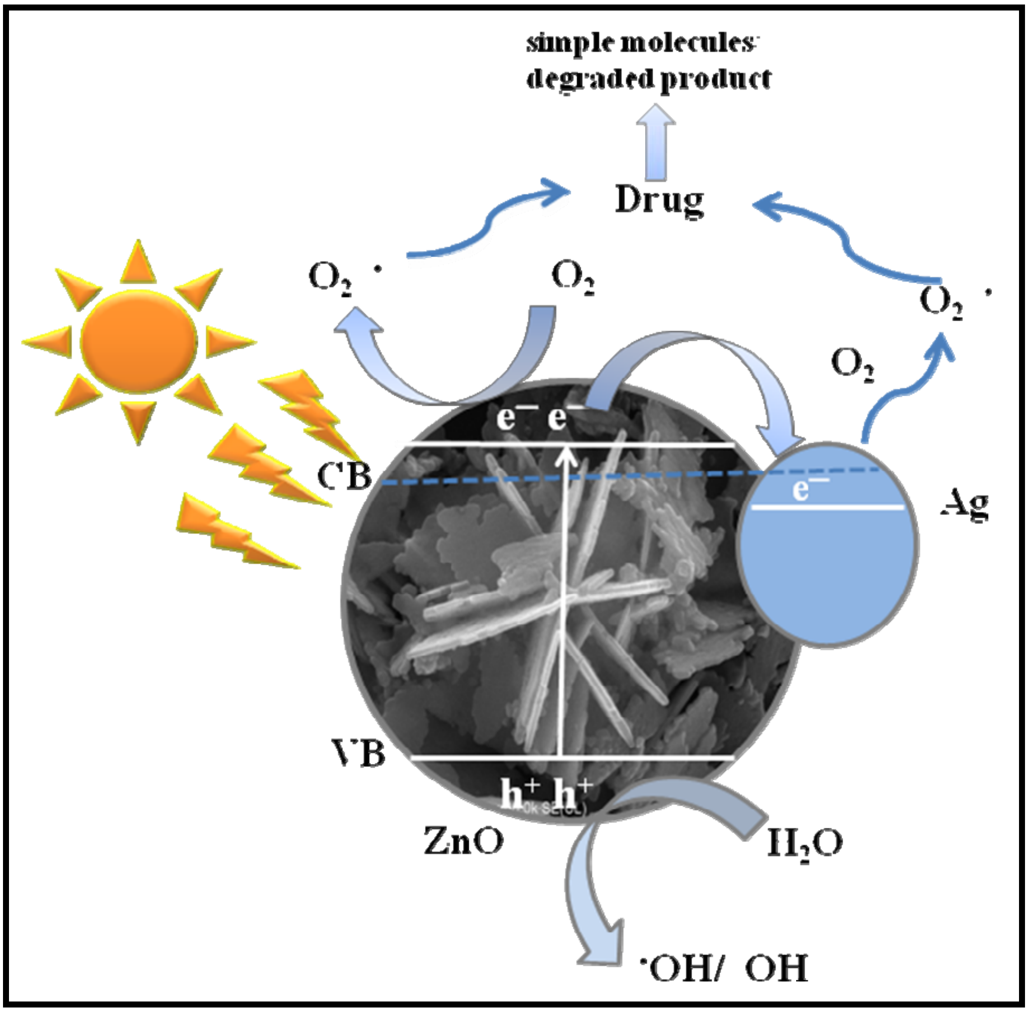

Fig. 7. Photocatalytic degradation mechanism over Ag-doped ZnO microplates under solar irradiation

$$ZnO + h\nu \longrightarrow ZnO\ (e^{-}_{CB} + h^{+}_{VB}) \quad (5)$$

$$Ag \longleftrightarrow Ag^{+} + e^{-}_{CB} \quad (6)$$

$$e^{-}_{CB} + O_2 \longrightarrow O_2^{\bullet -} \quad (7)$$

$$ZnO\ (h^{+}_{VB}) + {}^{-}OH/H_2O \longrightarrow {}^{\bullet}OH + H^{+} \quad (8)$$

$${}^{\bullet}OH + \text{drug compound} \longrightarrow CO_2 + H_2O + \text{other simple molecules /degraded products} \quad (9)$$

4. Conclusions

Ag-doped ZnO microplates have been synthesized using pH-mediated precipitation technique and typified in terms of their structural, morphological and optical properties. The as-synthesized Ag-doped ZnO microplates were employed as an potent photocatalyst and about 91% degradation of KTC was achieved in 110 minutes under solar light. The Ag-doped ZnO photocatalyst also exhibited better photodegradation efficiency as compared to pristine ZnO (71%). The enhanced photocatalytic efficiency of prepared photocatalyst is due to the formation of barrier in ZnO interface and Ag dopant. Meanwhile, Ag dopant acts as electron acceptor and the electrons moved from conduction band of ZnO to new formed interface and thereby decreases the $e^{-} + h^{+}$ recombination.

Acknowledgement

The authors greatly acknowledge the TEQIP-II grant of Dr S. S. Bhatnagar UICET, Panjab University, Chandigarh for funding.

References

[1] T. Mahvelati-Shamsabadi, E. K. Goharshadi, Photostability and visible-light-driven photoactivity anhancement of hierarchical ZnS nanoparticles: The role of embedment of stable defect sites on the catalyst surface with the assistant of ultrasonic waves, Ultrason. Sonochem. 34 (2017) 78-89.

[2] S. Sood, A. Umar, S. K. Mehta, S. K. Kansal, α-Bi_2O_3 nanorods: An efficient sunlight active photocatalyst for degradation of rhodamine B and 2.4.6-trichlorophenol, Ceram. Int. 41 (2015) 3355-3364.

[3] X. Li, J. Xia, W. Zhu, J. Di, B. Wang, S. Yin, Z. Chen, H. Li, Facile synthesis of few-layered MoS_2 modified BiOI with enhanced visible-light photocatalytic activity, Colloids Surf., A 511 (2016) 1-7.

[4] X. Li, Z. Hu, J. Liu, D. Li, X. Zhang, J. Chen, J. Fang, Ga doped ZnO photonic crystals with enhanced photocatalytic activity and its reaction mechanism, Appl. Catal. B: Environ. 195 (2016) 29-38.

[5] A. Kaur, S. K. Kansal, Bi_2WO_6 nanocuboids: An efficient visible light active photocatalyst for the degradation of levofloxacn drug in aqueous phase, Chem. Eng. J. 302 (2016) 194-203.

[6] J. Su, L. Zhu, P. Geng, G. Chen, Self-assembly graphitic carbon nitride quantum dots anchored on TiO_2 nanotube arrays: An efficient heterojunction for pollutants degradation under solar light, J. Hazard Mater. 316 (2016) 159-168.

[7] A. H. Ali, S. Kapoor, S. K. Kansal, Studies on the photocatalytic decolorization of pararosanilne chloride dye and its simulated dyebath effluent, Desalin. Water Treat. 25 (2011) 268-275.

[8] Y. Wang, X. Li, G. Lu, G. Chen, Y. Chen, Synthesis and photo-catalytic degradation property of nanostructured-ZnO with different morphology, Mater. Lett. 62 (2008) 2359-2362.

[9] B. Subash, B. Krishankumar, M. Swaminathan, M. Shanthi, Synthesis and characterization of cerium-silver co-doped zinc oxide as a novel sunlight-driven photocatalyst for effective degradation of reactive red 120 dye, Mater. Sci. Semicond. Process. 16 (2013) 1070-1078.

[10] O. F. Lopes, K. T. G. Carvalho, G. K. Macedo, V. R. de Mendonca, W. A. Jr, C. Rieiro, Synthesis of $BiVO_4$ via oxidant peroxo-method: insights into the photocatalytic performance and degradation mechanism of pollutants, New. J. Chem. 39 (2015) 6231-6237.

[11] K. Yao, P. Basnet, H. Sessions, G. K. Larsen, S. E. H. Murph, Y. Zhao, Fe_2O_3-TiO_2 core-shell nanorod arrays for visible light photocatalytic applications, Catal. Today 270 (2016) 51-58.

[12] X. Chong, B. Zhao, R. Li, W. Ruan, X. Yang, Photocatalytic degradation of rhodamine 6G on Ag modified TiO2 nanotubes: surface-enhanced Raman scattering study on catalytic kinetics and substrate recyclability, Colloids Surf., A 481 (2015) 7-12.

[13] P. Kundu, P. A. Deshpande, G. Madras, N. Ravishankar, Nanoscale ZnO/CdS heterostructures with engineered interfaces for high photocatalytic activity under solar radiation, J. Mater. Chem. 21 (2011) 4209-4216.

[14] S.-M. Lam, J.-C. Sin, A. Z. Abdullah, A. R. Mohamed, Transition metal oxide loaded ZnO nanorods: preparation, characterization and their UV-vis photocatalytic activities, Sep. Purif. Technol. 132 (2014) 378-387.

[15] Q. Yu, L. Jiang, T. Ai, Fabrication and characterization of Au-doped ZnO nanocandles synthesized on diamond film, Mater. Lett. 152 (2015) 142-144.

[16] B. Li, Y. Wang, Synthesis, microstructure, and photocatalysis of ZnO/CdS nano-heterostructure, J. Phys. Chem. Solids 72 (2011) 1165-1169.

[17] R. Chauhan, A. Kumar, R. P. Chaudhary, Photocatalytic studies of silver doped ZnO nanoparticles synthesized by chemical precipitation method. J. Sol-Gel Sci. Technol. 63 (2012) 546-553.

[18] A. Hui, J. Liu, J. Ma, Synthesis and morphology-dependent antimicrobial activity of cerium doped flower-shaped ZnO crystallites under visible-light irradiation, Colloids Surf., A 506 (2016) 519-525.

[19] Y. Yan, M. M. Al-Jassim, S.-H. Wei, Doping of ZnO by group-IB elements, Appl. Phys. Lett. 89 (2006) 181912 (1-3).

[20] B. S. Reddy, S. V. Reddy, N. K. Reddy, J. P. Kumari, Synthesis, structural, optical properties and antibacterial activity of co-doped (Ag, Co) ZnO nanoparticles, Res. J. Mater. Sci. 1 (2013) 11-20.

[21] R. Lamba, A. Umar, S. K. Mehta, W. A. Anderson, S. K. Kansal, Visible-light-driven photocatalytic properties of self assembled cauliflower-like AgCl/ZnO hierarchical nanostructures, J. Mol. Catal. A: Chem. 408 (2015) 189-201.

[22] A. Kaur, S. K. Kansal, Degradation of ofloxacin in aqueous phase using TiO_2/ZnO, J. Nanosci. Nanotechnol.-Asia 6 (2016) 113-118.

[23] F. Khan, S.-H. Baek, J. H. Kim, Enhanced charge transport properties of Ag and Al co-doped ZnO nanostructures via solution process, J. Alloys Compd. 682 (2016) 232-237.

[24] O. Lupan, L. Chow, L. K. Ono, B. R. Cuenya, G. Chai, H. Khallaf, S. Park, A. Schulte, Synthesis and Characterization of Ag- or Sb-doped ZnO nanorods by facile hydrothermal route, J. Phys. Chem. C 114 (2010) 12401-12408.

[25] S. Sood, A. Umar, S. K. Mehta, S. K. Kansal, Highly effective Fe-doped TiO_2 nanoparticles photocatalysts for visible light driven photocatalytic degradation of toxic organic compounds, J. Colloid Interface Sci. 450 (2015) 213-223.

[26] A. Kaur, A. Umar, S. K. Kansal, Sunlight-driven photocatalytic degradation of non-steroidal anti-inflammatory drug based on TiO_2 quantum dots, J. Colloid Interface Sci. 459 (2015) 257-263.

[27] R. Lamba, A. Umar, S. K. Mehta, S. K. Kansal, Sb_2O_3-ZnO nanospindles: A potential material for photocatalytic and sensing applications, Ceram. Int. 41 (2015) 5419-5438.

[28] W. Raza, M. M. Haque, M. Muneer, Synthesis of visible light driven ZnO: Characterization and photocatalytic performance, Appl. Surface Sci. 322 (2014) 215-224.

[29] K. C. Barick, M. Aslam, V. P. Dravid, D. Bahadur, Self-aggregation and assembly of size-tunable transition metal doped ZnO nanocrystals, J. Phys. Chem. C 112 (2008) 15163-15170.

[30] G. Murugadoss, Synthesis and characterization of transition metals doped ZnO nanorods, J. Mater. Sci. Technol. 28 (2012) 587-593.

[31] Z. Han, L. Ren, Z. Cui, C. Chen, H. Pan, J. Chen, Ag/ZnO flower heterostructures as a visible-light driven photocatalyst via surface plasmon resonance, Appl. Catal. B: Environ. 126 (2012) 298-305.

[32] L. Shi, L. Liang, J. Ma, Y. Meng, S. Zhong, F. Wang, J. Sun, Highly efficient visible light-driven Ag/AgBr/ZnO composite photocatalyst for degrading rhodamine B, Ceram. Int. 40 (2014) 3495-3502.

[33] L. Ye, J. Liu, C. Gong, L. Tian, T. Peng, L. Zan, Two different roles of metallic Ag on Ag/AgX/BiOX (X = Cl, Br) Visible light photocatalysts: surface plasmon resonance and Z-scheme bridge, ACS Catal. 2 (2012) 1677-1683.

[34] P. Carvalho, P. Sampaio, S. Azevedo, C. Vaz, J. P. Espinos, V. Teixeira, J.O. Carneiro, Influence of thickness and coating morphology in the antimicrobial performance of zinc oxide coatings, Appl. Surface Sci. 307 (2014) 548-557.

[35] T. N. Ravishankar, K. Manjunatha, T. Ramakrishnappa, G. Nagaraju, D. Kumar, S. Sarakar, B. S. Anandkumar, G. T. Chandrappa, V. Reddy, J. Dupont, Comparison of the photocatalytic degradation of trypan blue by undoped and silver-doped zinc oxide nanoparticles, Mater. Sci. Semicond. Process 26 (2014) 7-17.

[36] E. Sumesh, M. S. Bootharaju, Anshup, T. Pradeep, A practical silver nanoparticle-based adsorbent for the removal of Hg^{2+} from water, J. Hazard Mater. 189 (2011) 450-457.

[37] R. Georgekutty, M. K. Serry, S. C. Pillai, A highly efficient Ag-ZnO photocatalyst: synthesis, properties and mechanism, J. Phys. Chem. C 112 (2008) 13563-13570.

[38] S. Kumar, V. Singh, A. Tanwar, Structural, morphological, optical and photocatalytic properties of Ag-doped ZnO nanoparticles, J. Mater. Sci.: Mater. Electron. 27 (2016) 2166-2173.

[39] S. H. Jeong, B. N. Park, S. B. Lee, J. H. Boo, Metal-doped ZnO thin films: synthesis and characterizations, Surf. Coat. Technol. 201 (2007) 5318-5322.

[40] J. Liqiang, Q. Yichun, W. Baiqi, L. Shudan, J. Baojiang, Y. Libin, F. Wei, F. Honggang, S. Jiazhong, Review on photoluminescence performance of nanosized semiconductor materials and its relationships with photocatalytic activity, Sol. Energy Mater. Sol. Cells 90 (2006) 1773-1787.

[41] P. Arsana, C. Bubpa, W. Sang-aroon, Photocatalytic activity under solar irradiation of silver and copper doped zinc oxide: photodeposition versus liquid impregnation methods, J. Appl. Sci 12 (2012) 1809-1816.

[42] M. A. Behnajady, N. Modirshahla, M. Shokri, A. Zeininezhad, H. A. Zamani, Enhanced photocatalytic activity of ZnO nanoparticles by silver doping with optimization of photodeposition method parameters, J. Environ. Sci. Health, Part A, 44 (2009) 666-672.

[43] R. Wang, J. H. Xin, Y. Yang, H. Liu, L. Xu, J. Hu, The characteristics and photocatalytic activities of silver doped ZnO nanocrystallites, Appl. Surface Sci. 227 (2004) 312-317.

[44] O. A. Yildirim, H. E. Unalan, C. Durucan, Highly efficient room temperature synthesis of silver doped zinc oxide (ZnO:Ag) nanoparticles: structural, optical and photocatalytic properties, J. Am. Ceram. Soc. 96 (2013) 766-773.

[45] I. Udom, Y. Zhang, M. K. Ram, E. K. Stefanakos, A. F. Hepp, R. Elzein, R. Schlaf, D. Y. Goswami, A simple photolytic reactor employing Ag-doped ZnO nanowires for water purification, Thin Solid Films 564 (2014) 258-263.

[46] F. Peng, H. Zhu, H. Wang, H. Yu, Preparation of Ag-sensitized ZnO and its photocatalytic performance under simulated solar light, Korean J. Chem. Eng. 24 (2007) 1022-1026.

[47] E. M. Rodriguez, G. Marquez, M. Tena, P. M. Alvarez, F. J. Beltran, Determination of main species involved in the first steps of TiO_2 photocatalytic degradation of organics with the use of scavengers: The case of ofloxacin, Appl. Catal. B: Environ. 178 (2015) 44-53.

[48] X. Xiao, R. Hu, C. Liu, C. Xing, C. Qian, X. Zuo, J. Nan, L. Wang, Facile large-scale synthesis of β-Bi_2O_3 nanospheres as a highly efficient photocatalyst for the degradation of acetaminophen under visible light irradiation, Appl. Catal. B: Environ. 140-141 (2013) 433-443.

[49] X. Wang, Y. Tang, Z. Chen, T. -T. Lim, Highly stable heterostructured Ag-AgBr/TiO_2 composite: a bifunctional visible-light active photocatalyst for destruction of ibuprofen and bacteria, J. Mater. Chem. 22 (2012) 23149-23158.

[50] K. K. Paul, R. Ghosh, P. K. Giri, Mechanism of strong visible light photocatalysis by Ag_2O-nanoparticle decorated monoclinic TiO_2 (B) porous nanorods, Nanotechnol. 27 (2016) 315703 (1-15).

[51] D. Zhang, Photocatalytic oxidation of organic dyes with nanostructured zinc dioxide modified with silver metals, Russ. J. Phys. Chem. 85 (2011) 1416-1422.

[52] K. M. Lee, C. W. Lai, K. S. Ngai, J. C. Juan, Recent developments of zinc oxide based photocatalyst in water treatment technology: a review, Water Res. 88 (2016) 428-448.